Sensor Fusion-Based Low-Cost Vehicle Localization System for Complex Urban Environments

Jae Kyu Suhr, *Member, IEEE*, Jeungin Jang, Daehong Min, and Ho Gi Jung, *Senior Member, IEEE*

***Abstract*—This paper proposes a sensor fusion-based low-cost vehicle localization system. The proposed system fuses a global positioning system (GPS), an inertial measurement unit (IMU), a wheel speed sensor, a single front camera, and a digital map via the particle filter. This system is advantageous over previous methods from the perspective of mass production. First, it only utilizes low-cost sensors. Second, it requires a low-volume digital map where road markings are expressed by a minimum number of points. Third, it consumes a small computational cost and has been implemented in a low-cost real-time embedded system. Fourth, it requests the perception sensor module to transmit a small amount of information to the vehicle localization module. Last, it was quantitatively evaluated in a large-scale database.**

***Index Terms*—Vehicle localization, sensor fusion, road marking, particle filter, GPS, IMU, digital map.**

I. Introduction

VEHICLE localization is a key component of both autonomous driving and advanced driver assistance systems (ADAS) [1]. Global navigation satellite systems (GNSS) are the most widely used vehicle localization method. However, they provide inaccurate results in urban canyons or tunnels where the GNSS signal is reflected or blocked [2]. To alleviate this drawback, the fusion of GNSS and dead reckoning (DR) has been utilized. However, due to the integration error of the DR, this approach provides unreliable results in a long GNSS outage, which frequently occurs in complex urban environments [3]. Recently, to overcome this problem, the combination of perception sensor and digital map has been extensively researched [3]–[26]. This approach recognizes various objects using perception sensors and matches them with a digital map in order to remove the GNSS and DR errors. In the digital map, objects perceivable by various sensors are usually represented by occupancy grid, elevation map, feature points, line segments, and so on.

Previous digital map and perception sensor-based vehicle localization methods are disadvantageous from a mass production perspective due to some of the following reasons. First, in terms of sensor cost, they rely on high-priced sensors such as a real time kinematic (RTK) global positioning system (GPS), high-precision inertial measurement unit (IMU), and multi-layer light detection and ranging (LIDAR). Second, in terms of digital map volume, they store various types of environmental information such as whole road surface intensity, detailed road marking shapes, 3D feature points and their descriptors. Third, in terms of computational cost, they repetitively project map information onto the acquired sensor output or match numerous features with those stored in the digital map. Forth, in terms of in-vehicle communication, a perception sensor module should transmit a large amount of data to a vehicle localization module such as a raw image, infrared reflectivity, road marking features, and 3D feature points and their descriptors. Last, in terms of performance evaluation, they have usually been tested in simple urban situations, not in complex urban environments.

To overcome these drawbacks, this paper proposes a novel system that precisely localizes the ego-vehicle in complex urban environments. The proposed system fuses GPS, IMU and a digital map along with lanes and symbolic road markings (SRMs) recognized by a front camera via the particle filter. This system has the following advantages over the previous methods from the perspective of mass production:

1) It utilizes only low-cost sensors: GPS, IMU, wheel speed sensor, and a single front camera.
2) It requires a low-volume digital map where lanes and SRMs are expressed by a minimum number of points.
3) It consumes a small computational cost because the relative distance to the driving lane, SRM type and location are simply compared with the digital map.
4) It requests the perception sensor module to transmit a small amount of information (relative distance to the driving lane, SRM type and location) to the vehicle localization module.
5) It was quantitatively evaluated using the database acquired during 105 km of driving for 6 hours in complex urban environments.

II. Related Research

Vehicle localization methods can mainly be categorized into GNSS-based, GNSS and DR-based, and perception sensor and

Manuscript received November 6, 2015; revised March 3, 2016 and June 13, 2016; accepted July 21, 2016. Date of publication August 19, 2016; date of current version May 1, 2017. This research was supported in part by the Intelligent Vehicle Commercialization Program (Sensor Fusion-based Low Cost Vehicle Localization, Grant No. 10045880) and in part by the MSIP (Ministry of Science, ICT and Future Planning), Korea, under the C-ITRC (Convergence Information Technology Research Center) (IITP-2016-H8601-16-1008) supervised by the IITP (Institute for Information & communications Technology Promotion). The Associate Editor for this paper was V. Punzo. *(Corresponding author: Ho Gi Jung.)*

J. K. Suhr is with Korea National University of Transportation, Chungju 380-702, South Korea.

J. Jang and D. Min are with WITHROBOT Inc., Seoul 333-136, South Korea.

H. G. Jung is with the Department of Information and Communications Engineering, Korea National University of Transportation, Chungju 380-702, South Korea (e-mail: hogijung@ut.ac.kr).

Color versions of one or more of the figures in this paper are available online at http://ieeexplore.ieee.org.

Digital Object Identifier 10.1109/TITS.2016.2595618

digital map-based approaches. As aforementioned, recently, the perception sensor and digital map-based approach has been widely researched. This approach utilizes various objects such as curbs [4], building facades [5], poles [6], guardrails [7], and road markings [3], [7]–[26]. Since this paper is concerned with the road markings, this section focuses on road marking-based methods. The road marking-based methods extract markings on road surfaces and match them with road markings stored in the digital map. Since road markings are visually distinctive and under government regulations, they can be reliably detected compared to other objects. However, the road markings should be manually or semi-automatically designated during the mapping procedure. These methods can be categorized into signal-level, feature-level, and symbol-level approaches.

The signal-level approach utilizes raw perception sensor data obtained from road surfaces. Mattern *et al.* [8] matches intensities of image pixels with a virtual road surface image produced from the digital map. Levinson *et al.* [9] compares infrared reflectivities of a multi-layer LIDAR with their means and standard deviations stored in the digital map. The feature-level approach uses road marking features extracted from raw perception sensor data. Hata and Wolf [10], Yoneda *et al.* [11], Kim *et al.* [12], and Suganuma and Uozumi [13] extract road marking features by comparing infrared reflectivities obtained by LIDARs with threshold values or neighboring reflectivities. Schreiber *et al.* [14] finds road marking features by applying the oriented matched filter to stereo camera-based free space. Deusch *et al.* [15] utilizes the maximally stable extremal regions to extract road marking features from a front camera's images. Jo *et al.* [3] apply the top-hat filter-based road marking extractor to bird's-eye view images. The signal-level and feature-level approaches require less effort to process the perception sensor outputs. However, the raw perception sensor data and road marking features have a large amount of information. Thus, these approaches usually require a high computational cost for the matching procedure, a large storage volume for the digital map, and a wide bandwidth for in-vehicle communication between the perception sensor and vehicle localization modules.

The symbol-level approach recognizes various types of road markings and matches them with the digital map. Lane markings are the most widely used symbols for vehicle localization. Nedevschi *et al.* [16], Lundgren *et al.* [7], Lee *et al.* [17], Jo *et al.* [18], Lu *et al.* [19], Gruyer *et al.* [20], Tao *et al.* [21], Kamijo *et al.* [22], and Heidenreich *et al.* [23] utilize various types of cameras to recognize lane markings in a parametric way. Since the lanes include insufficient information for longitudinal localization, stop-lines and crosswalks have been utilized as well. Nedevschi *et al.* [16] and Marita *et al.* [24] detect stop-lines using a stereo camera and Jo *et al.* [18] detect crosswalks using a front camera. Although SRMs such as arrows and characters include both lateral and longitudinal position information, they are seldom used for localization purposes. Nedevschi *et al.* [16] detect five types of arrows for vehicle localization. But arrows are not fully utilized for estimating precise vehicle locations but only for recognizing the driving lane. Ranganathan *et al.* [25] and Wu and Ranganathan [26] localize the ego-vehicle by recognizing ten types of arrows and characters. Since SRMs are represented by contours with multiple points, this method requires extra efforts to match them with outlier-contaminated feature points and the digital map needs a large volume to store them. Although the symbol-level approach requires additional computing resources to recognize specific symbols, the cost is expected to be negligible because this function will be implemented as a part of a multi-functional front camera module that already has enough computing resources to conduct various tasks such as lane, vehicle, pedestrian, and traffic sign detection.

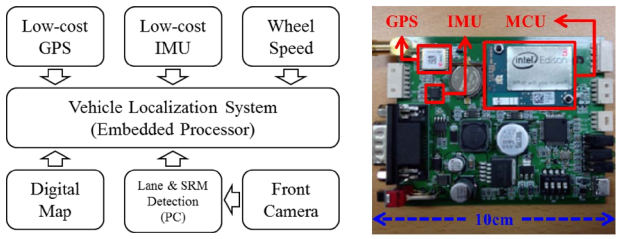

(a) (b)

Fig. 1. (a) Block diagram of the proposed system. (b) Embedded board developed by the authors.

III. System Overview

Fig. 1(a) shows the block diagram of the proposed vehicle localization system. This system utilizes a low-cost GPS, low-priced IMU, built-in wheel speed sensor, single front camera, and digital map. The proposed system fuses the digital map and outputs of various sensors based on the particle filter. The time update step predicts the distribution of the vehicle state using the IMU and wheel speed sensor, and the measurement update step corrects the vehicle position distribution using the GPS, front camera, and digital map [3]. The particle filter-based sensor fusion is conducted on an embedded processor in real-time. Currently, the lane and SRM detection runs on a PC. In case of mass production, this procedure will be implemented as a part of the multi-functional front camera module and only its outputs will be transmitted to the vehicle localization module. Fig. 1(b) shows the embedded board that conducts the proposed vehicle localization method. This board includes a GPS, IMU, and microcontroller unit (MCU), and its size is 10 cm by 7 cm. The cost of this board is less than 125 USD for individual purchase and a quantity purchase will lead to a significant cost reduction. The front camera is utilized to detect lanes and SRMs located within 20 m. Its resolution, field of view, and acquisition frequency are 752 $\times$ 480 pixels, 60° $\times$ 40°, and 20 Hz, respectively. Acquisition frequencies of the low-cost GPS, IMU, and wheel speed sensor are 1 Hz, 100 Hz, and 100 Hz, respectively.

IV. Map Building

The digital map was built by HYUNDAI MnSOFT, a company specializing in map-making, using a mobile mapping system (MMS) [27]. The MMS is composed of two high performance LIDARs, four high resolution cameras, an RTK-GPS, high precision IMU, and distance measurement indicator (DMI). The digital map was made by using the map building tool of the

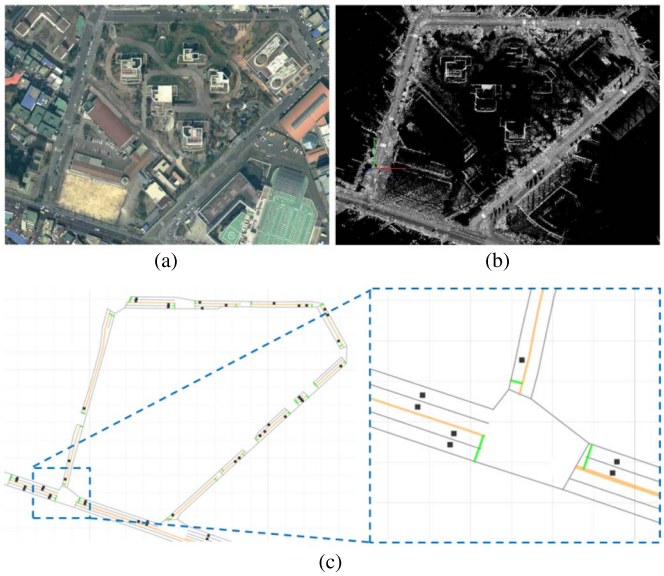

Fig. 2. Example of the digital map. (a) Satellite image of the area of interest. (b) Three-dimensional point clouds obtained by the MMS. (c) Generated digital map.

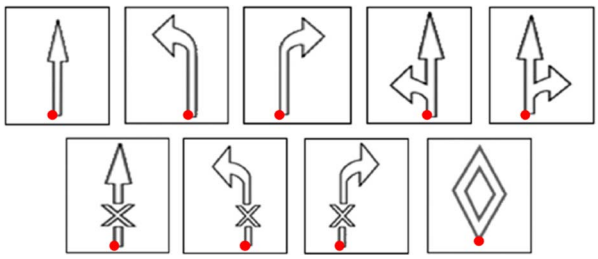

Fig. 3. Nine types of SRMs stored in the digital map. Red points indicate the SRM locations saved in the digital map.

HYUNDAI MnSOFT. Fig. 2 shows an example of the digital map. In this figure, (a) is a satellite image of the area of interest, (b) shows the 3D point clouds acquired by the MMS at (a), and (c) is a generated digital map from (b). The digital map includes lane and SRM information. To minimize its volume, detailed shapes and contours of the lanes and SRMs are not stored, but they are represented by minimum number of points. A lane is expressed by multiple points and the number of points depends on the road curvature. An SRM is represented by a single point. In Fig. 2(c), lines and points indicate lanes and SRMs, respectively. This digital map includes the nine types of SRMs shown in Fig. 3. In this figure, red points on the SRMs indicate the locations stored in the digital map.

V. Symbolic Road Marking Detection

This paper has extended the SRM detection method in our previous paper [28] to recognize not only SRMs on the driving lane but also those on the lanes next to it.

A. Lane Detection

In this paper, lane detection results have two purposes: one is to limit the search range of the SRM detection, and the other is to calculate the lateral position of the ego-vehicle in the driving lane. For these purposes, it is enough to detect the lanes located close to the ego-vehicle using a pair of straight lines. A top-hat filter $(\mathbf{f})$ is utilized to extract lane markings [29].

$$\mathbf{f} = [-\mathbf{1}_s \quad \mathbf{1}_{2s} \quad -\mathbf{1}_s] \tag{1}$$

where $\mathbf{1}_n$ indicates an n-dimensional row vector whose elements are all ones. The response of this filter (r) can efficiently be calculated using only four operations when using a horizontal integral image (I) as

$$r = 2\{I(x+s) - I(x-s)\} - \{I(x+2s) - I(x-2s)\}. \tag{2}$$

The width of the top-hat filter (s) changes according to the vertical coordinate in the image. These width values are precalculated based on the camera's intrinsic and extrinsic parameters and the lane width in the regulation. The inner pixels of the lane markings are extracted from the top-hat filtered image and applied to a RANSAC-based line estimator to detect a pair of straight lines. Fig. 4(a) shows an example result of lane detection with red lines. The top-hat filter was chosen because it produces a reasonable detection rate at a small computational cost.

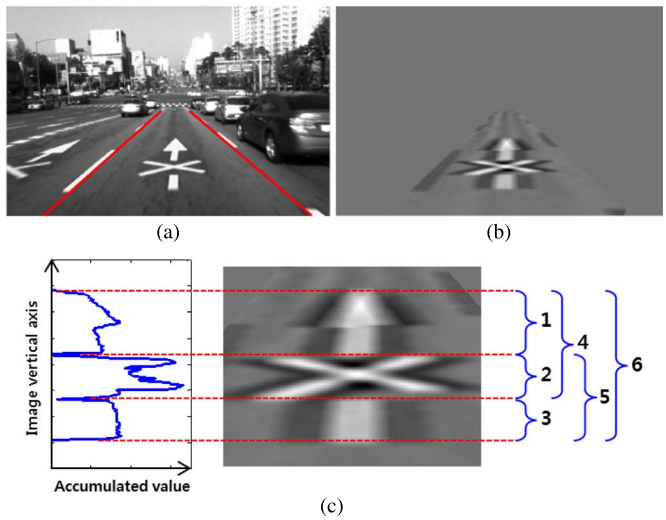

Fig. 4. SRM candidate generation procedure. (a) Lane detection result. (b) Top-hat filter response. (c) Projection histogram and SRM candidates.

B. SRM Candidate Generation

SRM candidates are generated using a projection histogram of the top-hat filtering result between two lanes. The top-hat filtering result is binarized and projected onto the image vertical axis. Fig. 4(b) and the left part of Fig. 4(c) show the top-hat filtering result and its projection histogram, respectively. Road marking blobs are extracted based on the changes of the projection histogram. In Fig. 4(c), three blobs are extracted. Since a single SRM may consist of multiple blobs, all blob combinations are generated as SRM candidates. In the case of Fig. 4(c), a total of six SRM candidates are generated. This approach can increase the SRM detection rate by creating at least one correctly generated SRM candidate even from damaged

or shadowed SRMs. The lane detection and SRM candidate generation procedures directly exploit original input images to save computational resources. Only the SRM candidate regions are converted into top-view images. To detect SRMs on the lanes next to the driving lane, the same procedure is applied to left and right lanes. Since the widths of those lanes are not measured in the image, they are assumed to be the same as the width of the driving lane.

C. SRM Classification

Once SRM candidates are generated, their types are determined using a histogram of oriented gradients (HOG) feature and total error rate (TER)-based classifier. HOG divides an image into multiple blocks that consist of several cells and describes the image using gradient-based histograms calculated from each cell [30]. A HOG feature is extracted from a top-view image of an SRM candidate. During the top-view image creation, the orientation of the SRM candidate is aligned to the longitudinal direction of the lanes. To determine the SRM type, this paper utilizes a TER-based classifier [31] whose learning procedure tries to minimize the summation of the false positive (FP) and false negative (FN) rates. This classifier was chosen because it can achieve both a high classification rate and low computational cost. In [28], the TER-based classifier shows a similar recognition rate as a support vector machine (SVM) with much faster computation time. TER can be calculated as

$$\text{TER} = \underbrace{\frac{1}{m^-}\sum_{j=1}^{m^-} L\left(g(\boldsymbol{\alpha}, \mathbf{x}_j^-) - \tau\right)}_{\text{FP}} + \underbrace{\frac{1}{m^+}\sum_{i=1}^{m^+} L\left(\tau - g\left(\boldsymbol{\alpha}, \mathbf{x}_i^+\right)\right)}_{\text{FN}} \tag{3}$$

where L is a zero-one step loss function, $g(\boldsymbol{\alpha}, \mathbf{x})$ is a classifier with adjustable parameters $\boldsymbol{\alpha}$ and feature vector $\mathbf{x}$. m and τ are sample number and threshold value, respectively, and the superscripts $+$ and $-$ denote the positive and negative samples, respectively. If a step function is approximated with a quadratic function and let $g(\boldsymbol{\alpha}, \mathbf{x}) = \mathbf{p}(\mathbf{x})\boldsymbol{\alpha}$, TER in (3) can be rewritten as

$$\text{TER} = \frac{b}{2}\|\boldsymbol{\alpha}\|_2^2 + \frac{1}{2m^-}\sum_{j=1}^{m^-}\left[\mathbf{p}\left(\mathbf{x}_j^-\right)\boldsymbol{\alpha} - \tau + \eta\right]^2 + \frac{1}{2m^+}\sum_{i=1}^{m^+}\left[\tau - \mathbf{p}\left(\mathbf{x}_i^+\right)\boldsymbol{\alpha} + \eta\right]^2 \tag{4}$$

where η is a positive offset of a quadratic function. $\mathbf{p}(\mathbf{x})$ is a reduced model (RM) of feature vector $\mathbf{x}$. RM is a reduced version of multivariate polynomial model [32]. $\boldsymbol{\alpha}$ that minimizes (4) can be calculated as

$$\boldsymbol{\alpha} = \left(b\mathbf{I} + \frac{1}{m^-}\mathbf{P}_-^T\mathbf{P}_- + \frac{1}{m^+}\mathbf{P}_+^T\mathbf{P}_+\right)^{-1} \times \left(\frac{(\tau-\eta)}{m^-}\mathbf{P}_-^T\mathbf{1}_- + \frac{(\tau+\eta)}{m^+}\mathbf{P}_+^T\mathbf{1}_+\right) \tag{5}$$

Fig. 5. Lane and SRM detection results.

where $\mathbf{I}$ is an identity matrix, and

$$\mathbf{P}_+ = \begin{bmatrix} \mathbf{p}\left(\mathbf{x}_1^+\right) \\ \mathbf{p}\left(\mathbf{x}_2^+\right) \\ \vdots \\ \mathbf{p}\left(\mathbf{x}_{m^+}^+\right) \end{bmatrix}, \quad \mathbf{P}_- = \begin{bmatrix} \mathbf{p}\left(\mathbf{x}_1^-\right) \\ \mathbf{p}\left(\mathbf{x}_2^-\right) \\ \vdots \\ \mathbf{p}\left(\mathbf{x}_{m^-}^-\right) \end{bmatrix},$$
$$\mathbf{1}_+ = \begin{bmatrix} 1 \\ \vdots \\ 1 \end{bmatrix} \Bigg\} m^+, \quad \mathbf{1}_- = \begin{bmatrix} 1 \\ \vdots \\ 1 \end{bmatrix} \Bigg\} m^-. \tag{6}$$

For efficient classification of the excessively generated SRM candidates, a cascade classifier composed of a two-class classifier and multi-class classifier is used. This method first utilizes a two-class classifier to rapidly reject non-SRM candidates, and then a multi-class classifier is only applied to the remaining candidates. Fig. 5 shows examples of the lane and SRM detection results. Red lines and yellow rectangles indicate the detected lanes and SRMs, respectively. Red points located at the bottoms of the yellow rectangles are the SRM locations stored in the digital map. This location is detected based on the intensity change at the bottom of the yellow rectangle. Once lanes and SRMs are detected, the lateral offset of the ego-vehicle with respect to the driving lane and the locations of the SRMs in 2D vehicle coordinates are calculated using the camera's intrinsic and extrinsic parameters.

VI. Vehicle Localization

This paper utilizes a particle filter to localize the ego-vehicle by fusing a GPS, IMU, front camera, and digital map [33]. The particle filter was chosen because it can fuse various sensors in a simple way, can produce reliable performance, and can be implemented in a low cost MCU.

A. Initialization and Time Update

Each particle $\mathbf{x}_t^n$ $(1 \le n \le N)$ is a concrete instantiation of the state at time t. n and N are an index and the number of particles, respectively. $\mathbf{x}_t^n$ is composed of 2D ego-vehicle location (x_t^n, y_t^n) and heading angle (θ_t^n) as

$$\mathbf{x}_t^n = \begin{bmatrix} x_t^n & y_t^n & \theta_t^n \end{bmatrix}^T. \tag{7}$$

Initial particles are generated based on the probability density function of the initial state, which is derived by the ego-vehicle position, velocity, and health status data provided by the GPS receiver. Predicted state $\hat{\mathbf{x}}_{t+1}$ is generated by the velocity motion model [33] as

$$\hat{\mathbf{x}}_{t+1}^n = \begin{bmatrix} \hat{x}_{t+1}^n \\ \hat{y}_{t+1}^n \\ \hat{\theta}_{t+1}^n \end{bmatrix} = \begin{bmatrix} x_t^n - \tilde{v}/\tilde{\omega}\sin(\theta) + \tilde{v}/\tilde{\omega}\sin(\theta + \tilde{\omega}\Delta t) \\ y_t^n + \tilde{v}/\tilde{\omega}\cos(\theta) - \tilde{v}/\tilde{\omega}\cos(\theta + \tilde{\omega}\Delta t) \\ \theta_t^n + \tilde{\omega}\Delta t + \tilde{\gamma}\Delta t \end{bmatrix}$$

$$\tilde{v} = v + \mathbf{sample}\left(\sigma_v^2\right),\ \tilde{\omega} = \omega + \mathbf{sample}\left(\sigma_\omega^2\right),$$

$$\tilde{\gamma} = \mathbf{sample}\left(\sigma_\gamma^2\right) \tag{8}$$

where $\tilde{\gamma}$ is an additional random term that perturbing the orientation and $\mathbf{sample}(\sigma^2)$ is a function that generates a random sample from a zero-mean Gaussian distribution with variance σ^2. v and ω are vehicle speed and yaw rate acquired from the built-in wheel speed sensor and IMU, respectively.

B. Measurement Update

In this paper, GPS and lane and SRM detection results along with the digital map are used for the measurement update. The final weight of the particle (w_t^n) is determined as

$$w_t^n = w_{t-1}^n \cdot w_{t,\mathrm{GPS}}^n \cdot w_{t,\mathrm{LANE}}^n \cdot w_{t,\mathrm{SRM}}^n \tag{9}$$

where $w_{t,\mathrm{GPS}}^n$, $w_{t,\mathrm{LANE}}^n$, and $w_{t,\mathrm{SRM}}^n$ are the weights obtained by the GPS, lane and SRM detection results, respectively. The weight of the unmeasured information at time t is set to 1. Once the final weights of all particles are calculated, their sum is normalized to 1.

A low-cost GPS usually shows poor localization accuracies in complex urban environments. The probability density distribution for the GPS-based measurement update is modeled by a multivariate Gaussian distribution with large variances as

$$w_{t,\mathrm{GPS}}^n = \frac{1}{2\pi\sqrt{\det(\Sigma_{\mathrm{GPS}})}} \times \exp\left\{-\frac{1}{2}\left(\hat{\mathbf{p}}_t^n - \mathbf{p}_{\mathrm{GPS}}\right)^T \Sigma_{\mathrm{GPS}}^{-1}\left(\hat{\mathbf{p}}_t^n - \mathbf{p}_{\mathrm{GPS}}\right)\right\} \tag{10}$$

where $\hat{\mathbf{p}}_t^n$ $(= [\hat{x}_t^n \quad \hat{y}_t^n]^T)$ is a 2D location of the predicted particle, and $\mathbf{p}_{\mathrm{GPS}}$ $(= [x_{\mathrm{GPS}} \quad y_{\mathrm{GPS}}]^T)$ is a 2D location measured by the GPS. Σ_{GPS} is a 2×2 diagonal matrix. The lane-based measurement update is conducted using the lane detection result. The lateral position of the ego-vehicle with respect to the driving lane (l_{LANE}) is calculated and compared with that of the predicted particle $(\hat{l}_t^n)$ as

$$w_{t,\mathrm{LANE}}^n = \frac{1}{\sqrt{2\pi\sigma_{\mathrm{LANE}}^2}} \exp\left\{-\left(\hat{l}_t^n - l_{\mathrm{LANE}}\right)^2 \Big/ 2\sigma_{\mathrm{LANE}}^2\right\} \tag{11}$$

$\hat{l}_t^n$ is calculated with respect to the lane in the digital map that includes the predicted particle $(\hat{\mathbf{x}}_t^n)$.

Once an SRM is detected, the same type of SRM is searched around the predicted ego-vehicle location in the digital map. If the same type of SRM is found in the digital map, the SRM-based ego-vehicle location $(\mathbf{p}_{\mathrm{SRM}})$ is calculated. This process is conducted using the absolute location of the matched SRM in the digital map and the relative position of the SRM measured by the SRM detection result, intrinsic and extrinsic parameters of the camera, and heading angle of the predicted particle. If multiple SRMs are concurrently detected in an input image, those SRMs are considered as a single set and the set composed of the same types of SRMs are searched in the digital map. In this case, $\mathbf{p}_{\mathrm{SRM}}$ is determined by averaging that of each SRM. The probability density distribution of the SRM-based measurement update is modeled by a multivariate Gaussian distribution as

$$w_{t,\mathrm{SRM}}^n = \frac{1}{2\pi\sqrt{\det\left(\mathbf{\Sigma}_{t,\mathrm{SRM}}^n\right)}} \times \exp\left\{-\frac{1}{2}\left(\hat{\mathbf{p}}_t^n - \mathbf{p}_{\mathrm{SRM}}\right)^T {\mathbf{\Sigma}_{t,\mathrm{SRM}}^n}^{-1}\left(\mathbf{p}_t^n - \mathbf{p}_{\mathrm{SRM}}\right)\right\} \tag{12}$$

where $\hat{\mathbf{p}}_t^n$ $(= [\hat{x}_t^n \ \ \hat{y}_t^n]^T)$ is a 2D location of the predicted particle, and $\mathbf{p}_{\mathrm{SRM}}$ $(= [x_{\mathrm{SRM}} \ \ y_{\mathrm{SRM}}]^T)$ is a 2D location measured by the SRM detection result. $\mathbf{\Sigma}_{t,\mathrm{SRM}}^n$ is a 2×2 covariance matrix.

C. Position Estimation and Resampling

The final position of the ego-vehicle is determined by the minimum mean square error (MMSE) estimator that can be approximated by the weighted mean of the particles. Resampling is conducted to prevent the situation where the probability mass is concentrated on a few particles. This paper utilizes a low-variance sampling method for resampling [33].

VII. Experiments

A. Experimental Environments

The proposed system was quantitatively evaluated using the database acquired in Seoul, South Korea. Seoul is the most heavily populated metropolitan area among the organization for economic co-operation and development (OECD) countries [34] and includes very complex and congested traffic conditions. Two different experimental routes in Seoul were established. Let us call these routes GANGBOOK and GANGNAM. The database was acquired by driving each route five times. The total driving length and time are 105 km and 6 hours, respectively. Fig. 6 show driving situations of the two experimental routes, respectively. GANGBOOK is approximately 8.5 km long and has at most 4 driving lanes in a single direction. Especially, this route includes 1 km-long road where the vehicle moves under an elevated railroad as shown in Fig. 6(a) with green arrowed lines. This road condition blocks or reflects the GPS signals. Maximum vehicle speed in this location was 60 km/h and driving times were between 20 and 30 minutes. GANGNAM is approximately 12.5 km long and has at most 7 driving lanes in a single direction. Especially, this route includes a 5 km-long road in urban canyons as shown in Fig. 6(b) with green arrowed lines and two tunnels whose lengths are about 300 m as shown in Fig. 6(b) with green rectangles. GPS

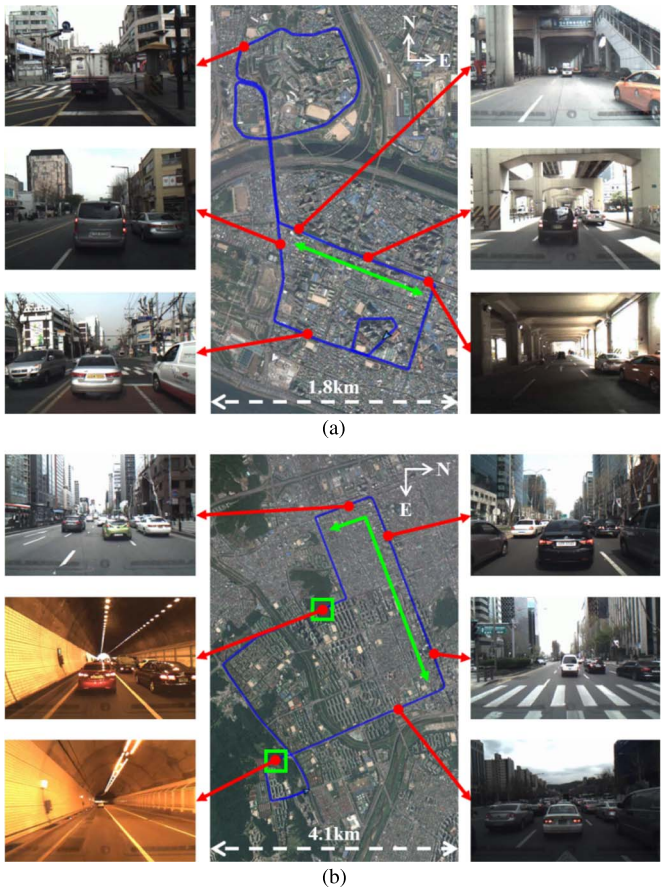

Fig. 6. Driving situations of two experimental routes. (a) GANGBOOK. (b) GANGNAM.

signals are blocked or reflected in these conditions. Maximum vehicle speed in this location was 75 km/h and driving times were between 35 and 60 minutes. Driving in GANGNAM took a long time due to many traffic lights and congested roads. The performance of the proposed system was quantitatively evaluated using Applanix POS-LV520 [35]. Its accuracy was evaluated based on the distance error between the location of the proposed system and that of Applanix POS-LV520.

B. SRM Detection Performance

The proposed system is robust against situations where an SRM is missed but relatively sensitive to situations where an SRM is falsely detected and matched. Thus, the proposed SRM detection is tuned to produce less false positives even though the detection rate is sacrificed. The proposed SRM detection method gives 60.97% recall and 99.45% precision in GANGBOOK and 64.69% recall and 100.00% precision in GANGNAM, respectively. Although this method achieves a moderate detection rate, it produces an extremely small number of false positives (only four false positives during 6 hours of driving). The two main reasons for missing SRMs are occlusions caused by other vehicles and unfavorable illumination conditions on SRMs.

TABLE I
LOCALIZATION PERFORMANCE IN GANGBOOK
[MEAN (STANDARD DEVIATION)]

DB	Proposed method [m]			GPS [m]		
	Lateral Error	Longitudinal Error	Euclidean Error	Lateral Error	Longitudinal Error	Euclidean Error
1	0.47 (0.47)	0.85 (0.87)	1.08 (0.86)	3.34 (2.88)	3.57 (3.62)	5.19 (4.29)
2	0.43 (0.43)	0.83 (0.78)	1.04 (0.77)	3.09 (4.23)	2.68 (7.01)	4.55 (7.95)
3	0.53 (0.61)	1.02 (0.90)	1.27 (0.95)	2.13 (3.08)	2.77 (4.84)	3.83 (5.52)
4	0.49 (0.51)	0.86 (0.80)	1.09 (0.83)	3.98 (6.25)	4.64 (8.94)	6.96 (10.38)
5	0.58 (0.64)	1.22 (1.23)	1.48 (1.25)	4.10 (11.01)	4.18 (10.10)	6.33 (14.74)
Total	**0.49 (0.53)**	**0.95 (0.92)**	**1.18 (0.94)**	**3.28 (5.92)**	**3.52 (7.18)**	**5.30 (9.04)**

TABLE II
LOCALIZATION PERFORMANCE IN GANGNAM
[MEAN (STANDARD DEVIATION)]

DB	Proposed method [m]			GPS [m]		
	Lateral Error	Longitudinal Error	Euclidean Error	Lateral Error	Longitudinal Error	Euclidean Error
1	0.36 (0.45)	1.42 (1.59)	1.56 (1.57)	7.37 (8.80)	11.23 (16.22)	14.71 (17.45)
2	0.67 (0.98)	1.02 (1.12)	1.38 (1.35)	9.11 (10.63)	6.05 (9.15)	12.75 (12.40)
3	0.72 (0.81)	1.53 (1.71)	1.89 (1.70)	10.81 (13.25)	7.80 (8.66)	14.00 (15.23)
4	0.60 (0.60)	1.42 (1.59)	1.68 (1.56)	8.81 (10.98)	10.79 (16.80)	16.19 (18.29)
5	0.51 (0.62)	1.69 (1.86)	1.88 (1.85)	11.53 (15.13)	6.45 (9.24)	14.10 (17.04)
Total	**0.58 (0.74)**	**1.43 (1.62)**	**1.69 (1.63)**	**9.65 (12.20)**	**8.34 (12.33)**	**14.26 (16.12)**

C. Vehicle Localization Performance

Tables I and II show the localization performances of the proposed system for 5 drives in GANGBOOK and GANGNAM, respectively. In these tables, lateral and longitudinal errors are the distance errors perpendicular and parallel to the heading of the ego-vehicle, respectively. In GANGBOOK, the proposed system gives 0.49 m lateral error, 0.95 m longitudinal error, and 1.18 m Euclidean error on average. The GPS provides 3.28 m lateral error, 3.52 m longitudinal error, and 5.30 m Euclidean error on average in the same condition. In GANGNAM, the proposed system gives 0.58 m lateral error, 1.43 m longitudinal error, and 1.69 m Euclidean error on average. The GPS provides 9.65 m lateral error, 8.34 m longitudinal error, and 14.26 m Euclidean error on average in the same condition.

Because a lane width in an urban area is wider than 3 m in South Korea, a lateral error less than 1.5 m means that an algorithm successfully recognizes driving lanes. In this sense, the proposed system succeeds in lane-level localization in 94.2% of GANGBOOK and 92.0% of GANGNAM. Additionally, assuming that a length of a mid-sized car is 5 m, the proposed system achieves localization accuracies of less than the length of the car in 99.4% of GANGBOOK and 94.8% of GANGNAM.

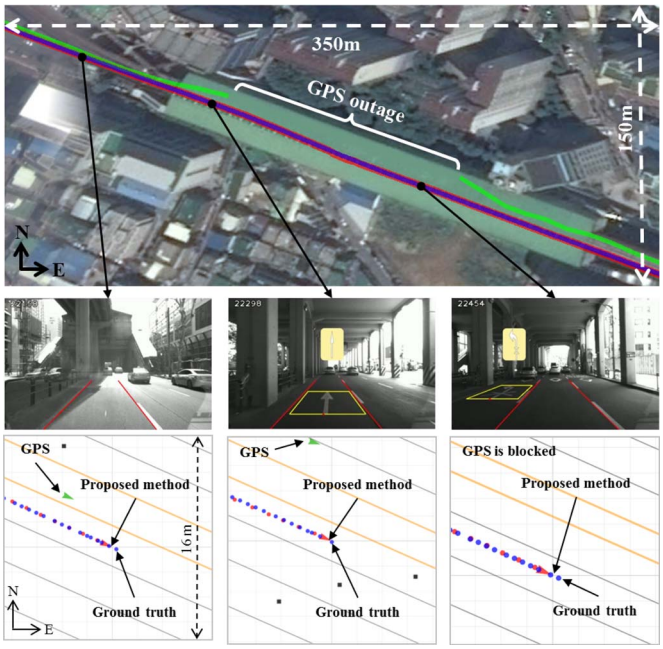

Fig. 7. Example of the localization result in GANGBOOK. In the upper image, blue, red, and green lines are the localization results obtained by the high-end localization system, proposed method, and GPS, respectively. In the middle image, red lines and yellow rectangles are the lane and SRM detection results, respectively. In the lower image, blue, red, and green points are detailed localization results of the high-end localization system, proposed method, and GPS, respectively.

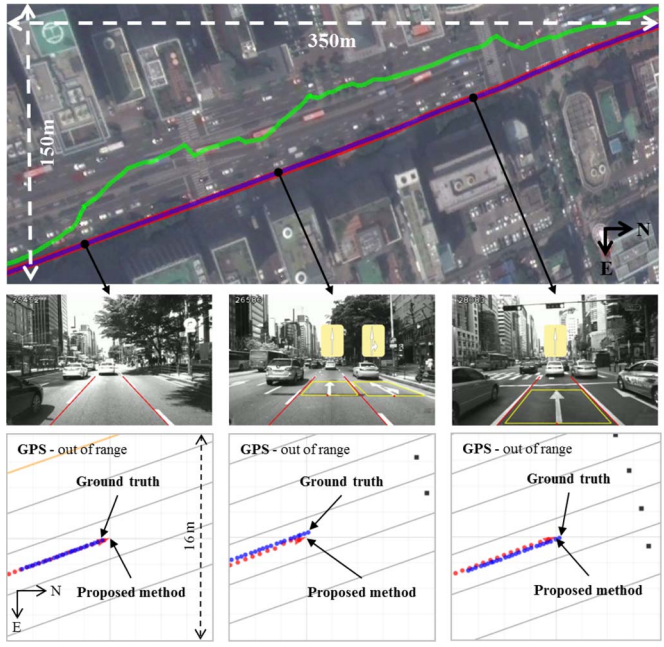

Fig. 8. Example of the localization result in GANGNAM. In the upper image, blue, red, and green lines are the localization results obtained by the high-end localization system, proposed method, and GPS, respectively. In the middle image, red lines and yellow rectangles are the lane and SRM detection results, respectively. In the lower image, blue, red, and green points are detailed localization results of the high-end localization system, proposed method, and GPS, respectively.

The longitudinal error of the proposed system is larger than its lateral error in both GANGBOOK and GANGNAM. This is because lateral positions can be updated by both lanes and SRMs but longitudinal positions can only be updated by SRMs, which are less frequently observed than lanes. GANGNAM has larger errors than GANGBOOK, mainly because of two reasons. One is that GANGNAM includes seven long road-segments (400∼600 m) where no SRM is presented while SRMs in GANGBOOK are more uniformly distributed. The other is that GANGNAM has a 5 km long road-segment in urban canyons but GANGBOOK has only a 1 km long road-segment under the elevated railroad.

Figs. 7 and 8 show examples of the localization results of the proposed system in GANGBOOK and GANGNAM, respectively. In these figures, the upper images are satellite pictures with trajectories of the localization results obtained by the high-end localization system (blue line), proposed method (red line), and GPS (green line). The middle images are the lane (red line) and SRM (yellow rectangle) detection results. The lower images are detailed localization results of the high-end localization system (blue point), proposed method (red arrow and point), and GPS (green arrow) in the digital map. Fig. 7 shows a situation where the ego-vehicle changes lanes under the elevated railroad. It can be seen that the GPS signals are completely blocked in the 120 m long road-segment. Fig. 8 shows a situation where the ego-vehicle keeps its driving lane in a long urban canyon. It can be seen that the GPS performance is severely affected by multipath propagation. Maximum Euclidean errors of the GPS in these two situations are approximately 8 m and 25 m, respectively. The localization results in these figures show that the proposed system can accurately localize the ego-vehicle in complex urban situations.

D. Execution Time

The lane and SRM detection currently runs on a PC (3.40 GHz Intel Core i7-2600 CPU with 8G RAM) because this procedure is assumed to be implemented as a part of the multi-functional front camera module in the case of mass production. The lane and SRM detection methods require 2 ms and 4 ms per frame, respectively. The particle filter-based vehicle localization runs on an embedded board with Intel Edison processor. This procedure is conducted at 100 Hz in the low-cost embedded board shown in Fig. 1(b).

E. Discussion

The localization error increases mainly in two cases. One is that no SRM is presented or detected in a long straight road. In this situation, the longitudinal error is getting larger because lanes update only lateral positions. The other is that the ego-vehicle passes through or turns in a large intersection. Since there is no lane marking and SRM inside the intersection area in South Korea, the ego-vehicle position is only updated by GPS and DR. This makes the localization error become larger while passing through large intersections. False detection of SRMs may also increase the localization error, but this rarely happened since the SRM detector was tuned to produce an extremely small number of false positives. Furthermore, falsely detected SRMs were not matched with SRMs in the digital map because the possibility that the same types of SRMs were presented around the predicted ego-vehicle locations is very low.

VIII. Conclusions and Future Work

This paper has proposed a low-cost precise vehicle localization system that fuses a GPS, IMU, wheel speed sensor, front camera, and digital map via the particle filter. From a mass production perspective, the proposed system is more adventurous than the previous methods in terms of sensor cost, digital map volume, computation cost, and in-vehicle communication. Furthermore, this system was implemented in a low-cost real time embedded system and quantitatively evaluated in complex urban environments. Experimental results have shown that this system reliably localizes the ego-vehicle even while passing through tunnels, long urban canyons, and under an elevated railroad.

References

[1] J. Ziegler *et al.*, "Making Bertha drive, an autonomous journey on a historic route," *IEEE Trans. Intell. Transp. Syst. Mag.*, vol. 3, no. 1, pp. 8–20, Summer 2014.

[2] S. Miura, L. T. Hsu, F. Chen, and S. Kamijo, "GPS error correction with pseudorange evaluation using three-dimensional maps," *IEEE Trans. Intell. Transp. Syst.*, vol. 16, no. 6, pp. 3104–3115, Dec. 2015.

[3] K. Jo, Y. Jo, J. K. Suhr, H. G. Jung, and M. Sunwoo, "Precise localization of an autonomous car based on probabilistic noise models of road surface marker features using multiple cameras," *IEEE Trans. Intell. Transp. Syst.*, vol. 16, no. 6, pp. 3377–3392, Dec. 2015.

[4] A. Y. Hata, F. S. Osorio, and D. F. Wolf, "Robust curb detection and vehicle localization in urban environments," in *Proc. IEEE Intell. Veh. Symp.*, Jun. 2014, pp. 1257–1262.

[5] L. Wei, C. Cappelle, and Y. Ruichek, "Horizontal/vertical LRFs and GIS maps aided vehicle localization in urban environment," in *Proc. IEEE Int. Conf. Intell. Transp. Syst.*, Oct. 2013, pp. 809–814.

[6] A. Schlichting and C. Brenner, "Localization using automotive laser scanners and local pattern matching," in *Proc. IEEE Intell. Veh. Symp.*, Jun. 2014, pp. 414–419.

[7] M. Lundgren, E. Stenborg, L. Svensson, and L. Hammarstrand, "Vehicle self-localization using off-the-shelf sensors and a detailed map," in *Proc. IEEE Intell. Veh. Symp.*, Jun. 2014, pp. 522–528.

[8] N. Mattern, R. Schubert, and G. Wanielik, "High-accurate vehicle localization using digital maps and coherency images," in *Proc. IEEE Intell. Veh. Symp.*, Jun. 2010, pp. 462–469.

[9] J. Levinson and S. Thrun, "Robust vehicle localization in urban environments using probabilistic maps," in *Proc. IEEE Int. Conf. Robot. Autom.*, May 2010, pp. 4372–4378.

[10] A. Y. Hata and D. F. Wolf, "Feature detection for vehicle localization in urban environments using a multilayer LIDAR," *IEEE Trans. Intell. Transp. Syst.*, vol. 17, no. 2, pp. 420–429, Feb. 2016.

[11] K. Yoneda, H. Tehrani, T. Ogawa, N. Hukuyama, and S. Mita, "Lidar scan feature for localization with highly precise 3-D map," in *Proc. IEEE Intell. Veh. Symp.*, Jun. 2014, pp. 1345–1350.

[12] D. Kim, T. Chung, and K. Yi, "Lane map building and localization for automated driving using 2D laser rangefinder," in *Proc. IEEE Intell. Veh. Symp.*, Jun. 2015, pp. 680–685.

[13] N. Suganuma and T. Uozumi, "Precise position estimation of autonomous vehicle based on map-matching," in *Proc. IEEE Intell. Veh. Symp.*, Jun. 2011, pp. 296–301.

[14] M. Schreiber, C. Knoppel, and U. Franke, "LaneLoc: Lane marking based localization using highly accurate maps," in *Proc. IEEE Intell. Veh. Symp.*, Jun. 2013, pp. 449–454.

[15] H. Deusch, J. Wiest, S. Reuter, D. Nuss, M. Fritzsche, and K. Dietmayer, "Multi-sensor self-localization based on maximally stable extremal regions," in *Proc. IEEE Intell. Veh. Symp.*, Jun. 2014, pp. 555–560.

[16] S. Nedevschi, V. Popescu, R. Danescu, T. Marita, and F. Oniga, "Accurate ego-vehicle global localization at intersections through alignment of visual data with digital map," *IEEE Trans. Intell. Transp. Syst.*, vol. 14, no. 2, pp. 673–687, Jun. 2013.

[17] Y.-C. Lee, Christiand, W. Yu, and J.-I. Cho, "Adaptive localization for mobile robots in urban environments using low-cost sensors and enhanced topological map," in *Proc. Int. Conf. Adv. Robot.*, Jun. 2011, pp. 569–575.

[18] K. Jo, K. Chu, and M. Sunwoo, "GPS-bias correction for precise localization of autonomous vehicles," in *Proc. IEEE Intell. Veh. Symp.*, Jun. 2013, pp. 636–641.

[19] W. Lu, E. Seignez, F. S. A. Rodriguez, and R. Reynaud, "Lane marking based vehicle localization using particle filter and multi-kernel estimation," in *Proc. Int. Conf. Control Automat. Robot. Vis.*, Dec. 2014, pp. 601–606.

[20] D. Gruyer, R. Belaroussi, and M. Revilloud, "Accurate lateral positioning from map data and road marking detection," *Expert Syst. Appl.*, vol. 43, no. 1, pp. 1–8, Jan. 2016.

[21] Z. Tao, P. Bonnifait, V. Fremont, and J. Ibanez-Guzman, "Lane marking aided vehicle localization," in *Proc. IEEE Int. Conf. Intell. Transp. Syst.*, Oct. 2013, pp. 1509–1515.

[22] S. Kamijo, Y. Gu, and L.-T. Hsu, "GNSS/INS/on-board camera integration for vehicle self-localization in urban canyon," in *Proc. Int. IEEE Conf. Intell. Transp. Syst.*, Sep. 2015, pp. 2533–2538.

[23] T. Heidenreich, J. Spehr, and C. Stiller, "LaneSLAM—Simultaneous pose and lane estimation using maps with lane-level accuracy," in *Proc. IEEE Int. Conf. Intell. Transp. Syst.*, Sep. 2015, pp. 2512–2517.

[24] T. Marita, M. Negru, R. Danescu, and S. Nedevschi, "Stop-line detection and localization method for intersection scenarios," in *Proc. Int. IEEE Conf. Intell. Comput. Commun. Process.*, Aug. 2011, pp. 293–298.

[25] A. Ranganathan, D. Ilstrup, and T. Wu, "Light-weight localization for vehicles using road markings," in *Proc. Int. IEEE/RSJ Conf. Intell. Robot. Syst.*, Nov. 2013, pp. 291–297.

[26] T. Wu and A. Ranganathan, "Vehicle localization using road markings," in *Proc. IEEE Intell. Veh. Symp.*, Jun. 2013, pp. 1185–1190.

[27] HYUNDAI MnSOFT, REAL, [Accessed: Nov. 2015]. [Online]. Available: https://www.youtube.com/watch?v=LAzX3zzvDV8

[28] J. K. Suhr and H. G. Jung, "Fast symbolic road marking and stop-line detection for vehicle localization," in *Proc. IEEE Intell. Veh. Symp.*, Jun. 2015, pp. 186–191.

[29] T. Veit, J.-P. Tarel, P. Nicolle, and P. Charbonnier, "Evaluation of road marking feature extraction," in *Proc. Int. Conf. Intell. Transp. Syst.*, Oct. 2008, pp. 174–181.

[30] N. Dalal and B. Triggs, "Histograms of oriented gradients for human detection," in *Proc. IEEE Comput. Vis. Pattern Recognit.*, Jun. 2005, pp. 886–893.

[31] K.-A. Toh and H.-L. Eng, "Between classification-error approximation and weighted least-squares learning," *IEEE Trans. Pattern Anal. Mach. Intell.*, vol. 30, no. 4, pp. 658–669, Apr. 2008.

[32] K.-A. Toh, Q.-L. Tran, and D. Srinivasan, "Benchmarking a reduced multivariate polynomial pattern classifier," *IEEE Trans. Pattern Anal. Mach. Intell.*, vol. 30, no. 4, pp. 740–755, Jun. 2004.

[33] S. Thrun, W. Burgard, and D. Fox, *Probabilistic Robotics*. Cambridge, MA, USA: MIT Press, 2005.

[34] OECD Statistics, *Population Density in Cities*, [Accessed: Nov. 2015]. [Online]. Available: http://stats.oecd.org/

[35] Applanix POS-LV520, [Accessed: Nov. 2015]. [Online]. Available: http://www.applanix.com/products/land/pos-lv.html

Jae Kyu Suhr (M'12) received the B.S. degree in electronic engineering from Inha University, Incheon, South Korea, in 2005 and the M.S. and Ph.D. degrees in electrical and electronic engineering from Yonsei University, Seoul, South Korea, in 2007 and 2011, respectively.

From 2011 to 2016, he was with the Automotive Research Center, Hanyang University, Seoul. He is currently a Research Professor with Korea National University of Transportation, Chungju, South Korea. His research interests include computer vision, image analysis, pattern recognition, and sensor fusion for intelligent vehicles.

Jeungin Jang received the B.S. and M.S. degrees in mechanical engineering from Konkuk University, Seoul, South Korea, in 2000 and 2002, respectively.

He is with WITHROBOT Inc., Seoul. His research interests include embedded systems, sensor fusion, localization, and navigation.

Daehong Min received the B.S. degree in control and instrumentation engineering from Korea University, Sejong, South Korea, in 2010 and the M.S. degree in control and instrumentation engineering from Korea University, Seoul, South Korea, in 2011.

He is a Software Engineer with WITHROBOT Inc., Seoul. His research interests include machine learning, computer vision, and sensor fusion.

Ho Gi Jung (M'05–SM'10) received the B.E., M.E., and Ph.D. degrees from Yonsei University, Seoul, South Korea, in 1995, 1997, and 2008, respectively, all in electronic engineering.

From 1997 to April 2009, he was with MANDO Corporation Global R&D Headquarters, where he developed environmental recognition systems for various driver assistant systems. From May 2009 to February 2011, he was with Yonsei University as a Full-Time Researcher and a Research Professor. From March 2011 to July 2016, he was with Hanyang University, Seoul, South Korea, as an Assistant Professor. Since August 2016, he has been an Associate Professor with the Department of Information and Communications Engineering, Korea National University of Transportation, Chungju, South Korea. He is working on recognition systems for intelligent vehicles. His research interests include recognition systems for intelligent vehicles, next-generation vehicles, computer vision applications, and pattern recognition applications.

Dr. Jung is an Associate Editor of IEEE TRANSACTIONS ON INTELLIGENT TRANSPORTATION SYSTEMS and IEEE TRANSACTIONS ON INTELLIGENT VEHICLES.